

Prediction of dispersed mineralization zone in depth using frequency domain of surface geochemical data

H. Shahi

Department of Mining Engineering, University of Gonabad, Gonabad, Iran

Received 2 August 2016; received in revised form 18 April 2017; accepted 5 May 2017
Corresponding author: *hssn.shahi@gmail.com (H. Shahi)*.

Abstract

Discrimination of the blind and dispersed mineralization deposits is a challenging problem in geochemical exploration. The frequency domain (FD) of the surface geochemical data can solve this important issue. This new exploratory information can be achieved using the interpretation of FD of geochemical data, which is impossible in spatial domain. In this research work, FD of the surface geochemical data is analyzed to decompose the complex geochemical patterns related to the mineral deposits. In order to identify the dispersed mineralization zone in the Chichakloo Pb–Zn deposit, a newly developed approach is proposed based on the coupling of two-dimensional Fourier transform (2DFT) and principal component analysis (PCA). The surface geochemical data is transferred to FD using 2DFT, and two low-pass filters are designed and performed on FD. Then the PCA method is employed on these frequency bands (FBs) separately. This proposed scenario desirably illustrates the relationship between the low frequencies in the surface geochemical distribution map (GDM) and the deep deposits. The informations obtained from the detailed exploration and the exploration drillings such as boreholes confirm the results obtained from this method. This new combined approach is a valuable data-processing tool and pattern-recognition technique in geochemical explorations. This approach is quite inexpensive compared to the traditional exploration methods.

Keywords: *Frequency Domain of Geochemical Data, Principal Component Analysis, Fourier Transformation, Dispersed Mineralization Zones, Pattern Recognition.*

1. Introduction

Distinguishing the blind and dispersed mineralization zones is an important issue in geochemical exploration. In general, two main methods have been applied to identify the presence or absence of mineral deposits beneath the ground surface. One approach employs the type of ore deposit and the other one is based upon its geochemical haloes [1]. The geochemical haloes of mineral deposits are related to the enrichment and depletion of elements [2-4] and/or mineral alterations [5-7].

Grigorian has presented a zonality model in the spatial domain (SD) of geochemical data to detect the blind mineralization zones from the dispersed mineralization zones [8, 9]. The zonality method assumes a linear relationship between the vertical

zonality coefficients and the depth of mineralization responses [10]. In addition to the zonality method, other methods have been applied to detect the hidden and dispersed ore deposits in SD of geochemical data based on the horizons of erosional surface [9, 11-14]. The variation in particular elements and their certain ratios in geochemical haloes of mineral deposits in SD can be used for vectoring toward the ore zones [15-17].

In addition to SD, the geochemical data can be interpreted in FD. The analysis of geochemical data in FD can provide new exploratory information that may not be exposed in SD [18-20]. Fourier transforms are widely used for many applications in engineering, science, and

mathematics. Fourier transforms are obtained by decomposing a sequence of values into components of different frequencies [21]. The power spectrum-area fractal method has been applied for separation of anomaly and background in FD of geochemical data [22-32]. Zuo and Wang have reviewed the fractal/multi-fractal models of geochemical data in SD and FD [33]. Wang and Zuo have presented a Matlab-based program for processing the geochemical data by means of the fractal/multi-fractal method in SD and FD [34]. Shahi et al. have demonstrated that there is a relationship between the frequencies of GDM and the depth of mineral deposits [18-20]. The geochemical migration process causes different geochemical haloes in the surface based on the depth of deposit. The deep ore deposits create low concentrations, and the shallow ore bodies may have large concentrations in the surface [35]. These haloes of mineral deposits and enrichment and depletion of elements at different depths affect different frequency distributions of elements in the surface. The very low frequencies are related to the background values and deep mineral deposits [18-20]. Shahi et al. have demonstrated that depletion and enrichment of particular elements in geochemical haloes of mineral deposits create different varieties of frequency distribution maps (FDMs) in surface geochemical data [20]. In this research work, in order to identify the Pb– Zn blind mineral deposit, a combined approach based on FD of surface geochemical data and PCA method is proposed.

2. Materials and methods

2.1. Case study

The Chichakloo area is located in the NW of Iran, SW of the city of Zanjan, 30 kilometers from Takab to the east (Figure 1). The studied area is located in the collision place of the two tectonic zones Alborz-Azerbaijan and Sanandaj-Sirjan. The oldest geological unit, aged Precambrian, includes mica and talc schist and outcrops in the south and west of the studied area. The second unit, aged Paleozoic, has been formed from gray-to white-colored dolomites that are occasionally brecciated. The brown dolomite is the oldest carbonate unit in the studied area. This unit contains chert bands, occasionally with silica veins and veinlets, which are increased toward the north in the studied area. This brown dolomite unit is overlain by grey to black dolomites of low to moderate thickness that are situated in immediate contact with the sand-breccia dolomite unit. This unit contains, as the host rock of lead and zinc ore deposit, a relatively high amount of fine white calamine in the middle and western parts of the studied area. One of the most important specifications of this unit is that it contains silica veins and veinlets and jasperoid bodies, and has an extensive spread in the western and north-western parts of the studied area. The youngest geological unit, aged Eocene, consists of sandstone and red-colored shale (Figure 2). Most of the faults in the area have a NS trend [36].

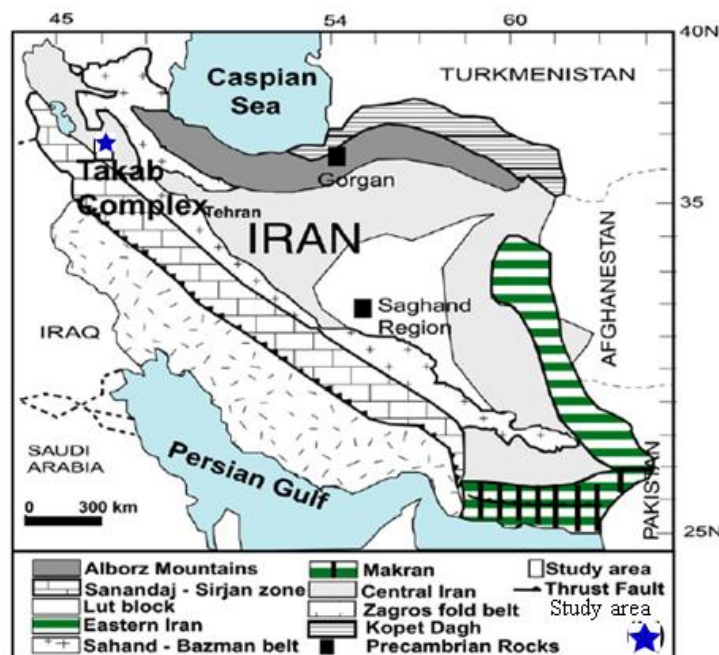


Figure 1. Chichakloo Pb-Zn mineralization area is located in NW of Iran [37].

The main controlling factors involved in the mineralization include the sand-breccia dolomite, the contact between dolomite and shale, and also the diagenetic processes in the lead and zinc mineralization of disseminated, laminated, and veinlet forms. Tectonic processes such as NS faults have a significant role in the re-placement of the metallic ores. Galena minerals re-grow inside the calcite and dolomite crystals, indicating

the simultaneous occurrence of the metallic ore and host rock minerals. Sphalerite and cubic pyrite are also observed with galena in the ore minerals. Lead and zinc primary minerals in the ground surface and shallow depth due to weathering and supergene processes have been converted to secondary minerals such as smithsonite, calamine, and cerosite [36].

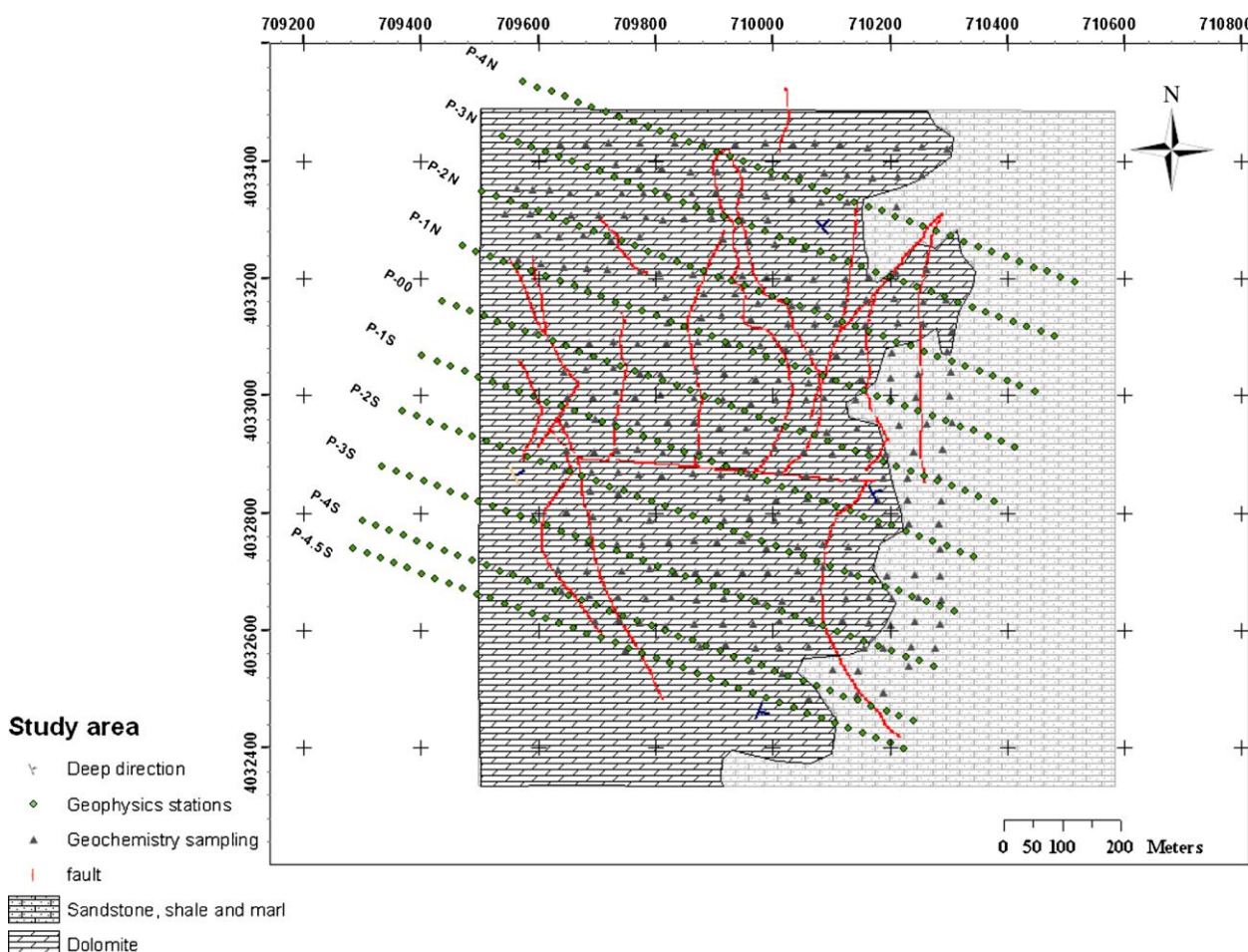


Figure 2. Geological map of studied area showing geological units, faults, parallel geophysical exploration stations, and grid net of geochemical sampling [36].

2.2. Fourier transform

The Fourier series show us how to decompose any periodic function to a sum of sinusoids. The Fourier transform is the extension of this idea to non-periodic functions. The Fourier transform decomposes any function into a sum of sinusoidal basis functions. Each of these basis functions is a complex exponential of a different frequency. Re-writing sinus and cosines as complex exponentials makes it necessary for the Fourier coefficients to be complex-valued. The usual interpretation of this complex number is that it gives both the amplitude of the wave present in the function and the phase (or the initial angle) of

the wave. The Fourier transform can measure the frequencies that are present in the original signal, and we can recombine these waves using an integral to reproduce the original function [38]. The Fourier method is the most powerful technique for signal analysis. It transforms the signal from time or spatial domain to FD in which many characteristics of the signal are revealed [26]. Fourier transformation is the mathematical procedure connecting $S(x)$ and $F(\omega)$. $S(x)$ is the 1D SD signal, and $F(\omega)$ is called the Fourier transform of $S(x)$ and the so-called FD representation. In general, $F(\omega)$ is a

complex-valued function composed of harmonic frequencies, phases, and their amplitudes obtained from the Fourier expansion. If $S(x)$ is specified, $F(\omega)$ may be computed, and vice versa. Here, the defining equations for completeness have simply been provided:

$$F(\omega) = \int_{-\infty}^{\infty} S(x) e^{-i\omega x} dx \quad (1)$$

$$S(x) = \frac{1}{2\pi} \int_{-\infty}^{\infty} F(\omega) e^{-i\omega x} d\omega \quad (2)$$

In the above-mentioned equations, ω is the fundamental frequency. Equation 1 is the Fourier transform and equation 2 is the inverse Fourier transform. Figure 3 simply illustrates the 1D Fourier transform. In this figure, the 1D signal in SD has been decomposed into its deferent main frequencies using Fourier transform, and subsequently, the signal has been shown in FD based on the amplitude and phase [39]. Fourier analysis converts a signal from its original domain (often time or space) to a representation in the FD, and vice versa [40].

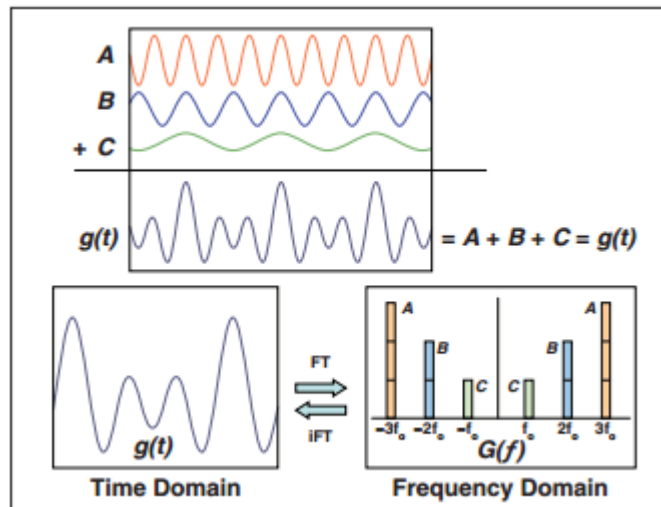


Figure 3. Schematic process of Fourier transformation of time (spatial) domain to frequency domain [41].

2DFT is a straightforward extension of the 1D Fourier transform. 2DFT allows us to represent and interpret the spatial data such as the images in FD [42]. The SD responses can be considered as superimposed signals of different frequencies [28]. One of the equations used for conducting the Fourier transform has been presented by Dobrin and Savit [43]:

$$F(K_x, K_y) = \int_{-\infty}^{\infty} \int_{-\infty}^{\infty} f(x, y) \cos(K_x x + K_y y) dx dy - i \int_{-\infty}^{\infty} \int_{-\infty}^{\infty} f(x, y) \sin(K_x x + K_y y) dx dy \quad (3)$$

where $f(x, y)$ is the signal in SD, and K_x and K_y are “wave numbers” with respect to the x and y axes, respectively. Wave number is the spatial counterpart of frequency, increasing proportionally to wavelengths as bellow:

$$\lambda_x = 2\pi / K_x \text{ and } \lambda_y = 2\pi / K_y, \quad \text{or} \quad \lambda = 2\pi \sqrt{(1/K_x^2 + 1/K_y^2)} \quad (4)$$

Therefore, a function $f(x, y)$ in SD, which is surface GDM in this study, can be converted into $F(K_x, K_y)$. It consists of the real and imaginary parts $R(K_x, K_y)$ and $I(K_x, K_y)$, respectively. The power spectrum is defined based on the following equation [44, 45]:

$$E(K_x, K_y) = R^2(K_x, K_y) + I^2(K_x, K_y) \quad (5)$$

The processing of geoscience data in FD often involves operations such as filtering and reducing the noise from signal [46]. The filter function, $G(K_x, K_y)$, can modify the functions $R(K_x, K_y)$ and $I(K_x, K_y)$ by multiplying so that some ranges of wave numbers can be eliminated and others enhanced. The conventional filters in physics, electrical engineering, and geophysics include low-pass, high-pass, band pass, and directional band pass filters [47]. A low-pass filter generally eliminates the signals with high frequencies, and a high-pass filter eliminates low frequencies. These filters may be performed on the K_x - K_y map only based on the wave number values without considering the power spectrum values [48].

2.3. Principal component analysis (PCA)

PCA can reduce the dimensionality of a dataset consisting of a large number of interrelated variables [49]. PCA can maximize the variance of a linear combination of the variables, and shows the data in different dimensions. Suppose that X is a vector of p original variables. Usually the original variables in X are correlated, and the distribution of points is not oriented parallel to any of the axes represented by X_1, X_2, \dots, X_p . PCA can find the directions of high variability of data as natural axes of the swarm of points. This is done by translating the origin data and rotating the axes. The new variables (principal components) will be uncorrelated after rotation [50]. The new variables obtained in the new coordinate system are uncorrelated, and the first PC contains the most variations in the original variables. PCA can find the few derived variables that represent most of the information given by variances and correlations or covariances. PCA is performed using the calculation of eigenvectors of the covariance matrix or correlation matrix on

original variables. The $p \times p$ correlation matrix for p variables has p eigenvalues and p eigenvectors (a_1, a_2, \dots, a_p). If the k -th eigenvector is $a_k = (a_{1k}, a_{2k}, \dots, a_{pk})$, then PCs Y_1, Y_2, \dots are calculated by:

$$\begin{cases} Y_1 = a_{11}X_1 + a_{21}X_2 + \dots + a_{p1}X_p \\ Y_2 = a_{12}X_1 + a_{22}X_2 + \dots + a_{p2}X_p \\ \dots \\ Y_p = a_{1p}X_1 + a_{2p}X_2 + \dots + a_{pp}X_p \end{cases} \quad (6)$$

The K th derived variable, Y_k , is the K th PC [49].

3. Results and discussion

A geochemical investigation was performed in a detailed exploration stage. In the geochemical study stage, 292 litho-geochemical samples were collected, and these samples were analyzed using the ICP method in Amdel Laboratory in Australia for 39 elements in the studied area. A blank sheet of sample location and concentration of Pb and Zn in this area are shown in Figure 4.

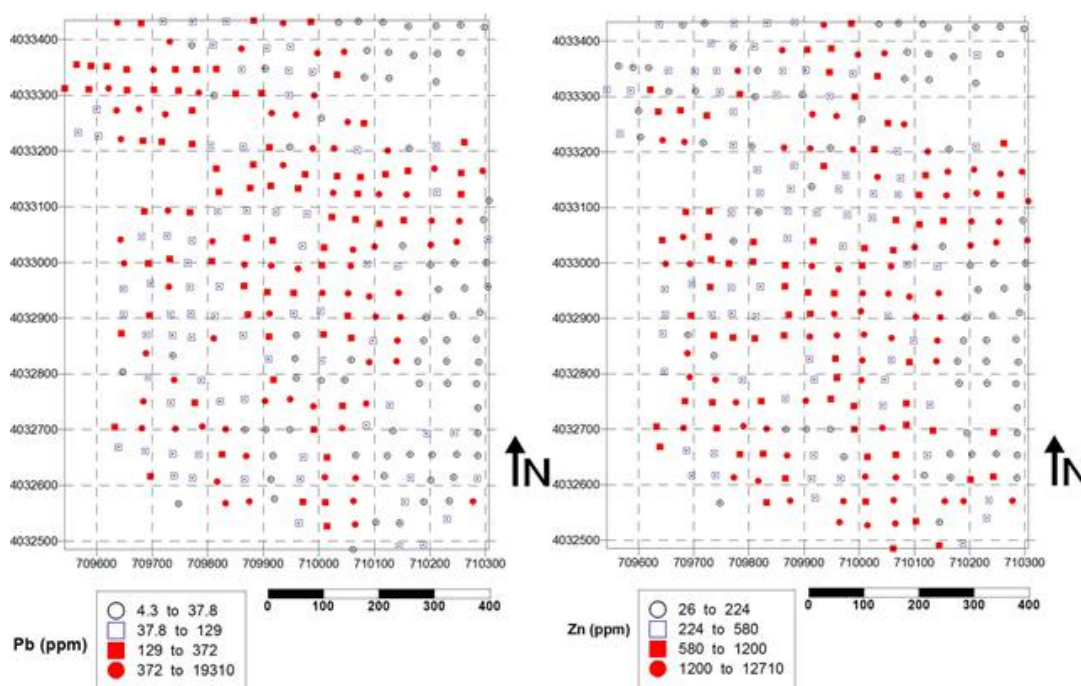


Figure 4. Blank sheet of sample location and concentration of Pb and Zn.

After data processing, multi-elemental analyses were carried out using PCA to determine the attributes of mineralization and recognize the chemical behavior of the paragenesis elements accompanying the main elements (i.e. Pb and Zn). PCA is a multivariate statistical method for geo-information identification of geo-datasets [51]. In the PCA method, correlated variables with high dimensionality are transformed into

several uncorrelated principal components (PCs) based on a covariance or correlation matrix [52]. The PCA method has been frequently applied for the analysis of geochemical and geoscience data [29, 47, 51, 53, 54]. In this work, PCA was performed on the litho-geochemical data in SD. The results obtained for PCA are shown in Table 1. The first four components represent about 77.5% of the total variance. The first PC (PC1) in

Table 1 can be attributed to the decomposition of syngenetic components. PC1 is related to geochemical background and syngenetic elements. In this factor, the high negative amounts of Ca and Mg are related to the dolomite host rock, while the high positive values for other elements are related to the sandstone unit. The high coefficients for the Zn, Pb, Au, Ag, As, Cu, Mo, Sb, Cd, and Tl elements seen in the second PC (PC2) indicate the paragenesis elements accompanying the Pb and Zn mineralization in the studied area. In order to determine the

mineralization and paragenesis elements, the numerical value of 0.5 was considered as a criterion in the rotated component matrix obtained from the PCA method. The mineralization principal component scores versus the elements are delineated in Figure 5, and the mineralization and paragenesis elements including Zn, Pb, Au, Ag, As, Cu, Mo, Sb, Cd, and Tl were separated from the other elements. The mineralization and paragenesis elements in the surface geochemical data have a proper relationship together, which is recognizable using the PCA method.

Table 1. Rotated component matrix obtained from PCA method–mineralization PC, and its elements have been highlighted (based on threshold of 0.5).

	Component			
	1	2	3	4
Au	-.131	.764	.018	.035
Cr	.709	.139	.039	-.322
Mn	.395	.044	.735	.222
Ni	.760	.268	.308	.083
Pb	-.364	.816	-.144	.137
Sr	.062	-.302	.729	-.205
Ba	.805	.135	.263	.029
Be	.805	-.165	.087	-.298
Ti	.968	-.147	.052	.051
Fe	.822	.348	.177	.013
Al	.928	-.142	.158	.125
Ca	-.941	-.020	.065	.123
Li	.850	.115	.128	.112
P	.922	.006	.118	.074
V	.975	-.054	.035	.026
Mg	-.931	.083	-.135	.111
K	.951	-.111	.024	.038
Na	.825	-.202	.172	.044
S	.246	.276	.019	.646
Zr	.855	-.167	.141	.171
Ag	.009	.850	-.107	-.039
As	-.224	.875	-.116	.051
Bi	.432	.496	.077	-.038
Co	.825	.225	.343	.082
Cu	.306	.733	.118	.106
Mo	.259	.619	.116	-.435
Sb	-.042	.905	-.084	.072
Zn	-.337	.730	-.166	.087
Sn	.897	.069	-.062	.056
W	.715	.161	.101	-.230
Cs	.919	-.078	.077	.043
Nb	.952	-.141	.062	.009
U	.738	.291	.064	-.022
Cd	-.564	.553	-.194	.228
Rb	.959	-.116	.064	.055
Th	.961	-.131	.122	.078
Y	.758	-.133	.298	-.089
Ce	.915	-.091	.100	.074
Tl	.419	.645	.199	-.045

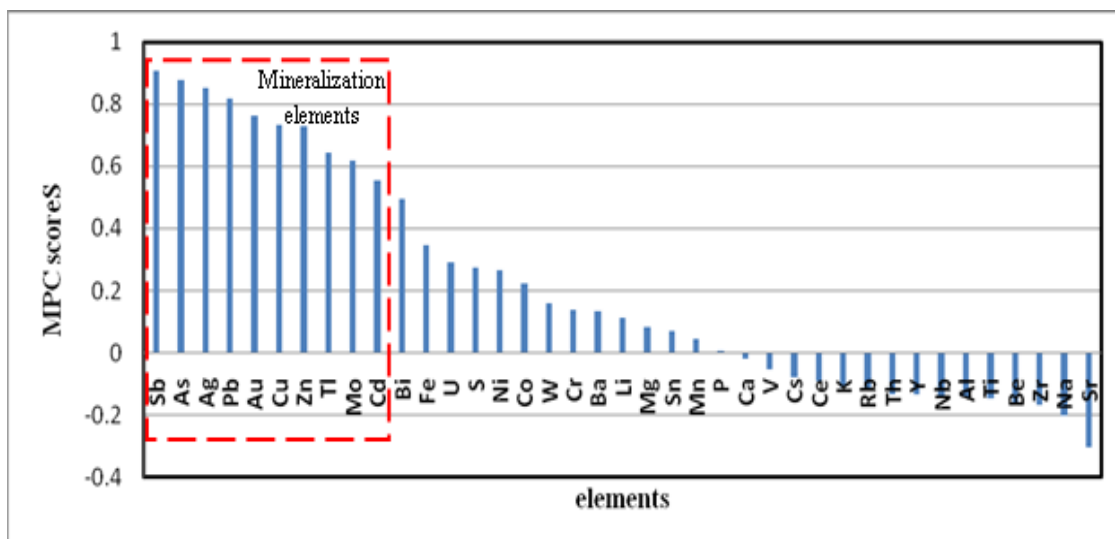


Figure 5. Mineralization and paragenesis elements and their scores in mineralization principal component (MPC).

The SD geochemical data for 39 elements were transferred to FD using 2DFT. The Fourier transform is called the FD representation of the original GDM. It is a mathematical approach that allows GDM to be decomposed into a sum of sine waves with different frequencies, phases, and amplitudes. This technique involves treating GDM as a 2D signal and applying standard signal-processing techniques to it. The Fourier transform separately decomposed these maps for 39 elements into different frequencies. The frequencies in FDM show the oscillations and variations in GDM of elements. The data in FD includes the wave numbers in the horizontal and vertical directions and their power spectrum values. GDM in SD and FDM in FD for Pb are shown in Figure 6. FDM obtained by Fourier transformation illustrates the high and low frequencies and distribution of power spectrum values in the studied area. In FD, we powered the spectrum values and wave numbers in the x and y directions instead of the elements of the geochemical map. High values of the power spectrum are mainly distributed around the center of the map corresponding to low frequencies. In general, the power spectrum values decrease, moving away from the center. The power spectrum contains no phase information from GDM as the original function. GDM of elements is a representation of a signal with perfect spatial resolution but no frequency information, while FDM of elements has perfect frequency resolution but no spatial information. The magnitude or power spectrum value of the Fourier transform at a point is how much the frequency content is there.

The patterns for FDMs in the surface mineral deposits are different from those for the deep mineral deposits. Analyzing the behavior of mineralization elements in low frequency bands can be suitable for interpretation of the presence or absence of deep ore deposits. The power spectrum of frequencies in FDM of elements is important in analyzing their properties.

The mineral deposits at different depths cause different GDMs in the surface. Therefore, the surface GDMs of mineralization elements include various frequencies in the surface. Interesting exploratory information can be achieved using the interpretation of frequency patterns in FDM of surface geochemical data.

In some complicated geological environments, extraction of exploratory features in SD is impossible but these patterns can be clearly concluded in FD. Different exploratory patterns can be identified using the frequency attributes of elements. The high frequencies in surface GDM of mineralization elements are related to the surface deposit and geochemical noises.

The blind and deep mineral deposits may create very weak and invisible geochemical effects in the surface GDM of elements, and their assays may be around the background values in the SD surface geochemical data. There is an inverse relationship between the depth of deposit and the frequencies of surface GDM. As the frequencies of surface GDM are reduced, the depth of mineralization is increased. The background patterns related to the regional geological processes and deep mineralization can create low frequencies in surface GDM. In the deep ore deposit, the paragenesis and mineralization

elements in the surface GDM have distinctive frequency patterns in low FBs. Therefore, PCA can be applied to low FBs to classify the low frequencies of elements in the background and deep deposits.

Two filter functions based on the wave numbers and power spectrum values were designed (Table 2). These low-pass filters were performed on FD of geochemical data for all elements. The Pb

power spectrum maps for FB1 and FB2 obtained from Pb GDM and their filter functions are depicted in Figure 7. Therefore, these filters were used based upon the wave number values in the x and y directions. In order to survey the mineralization features and determine the elements related to mineralizing phase in the depth, the PCA method was separately performed on two low FBs.

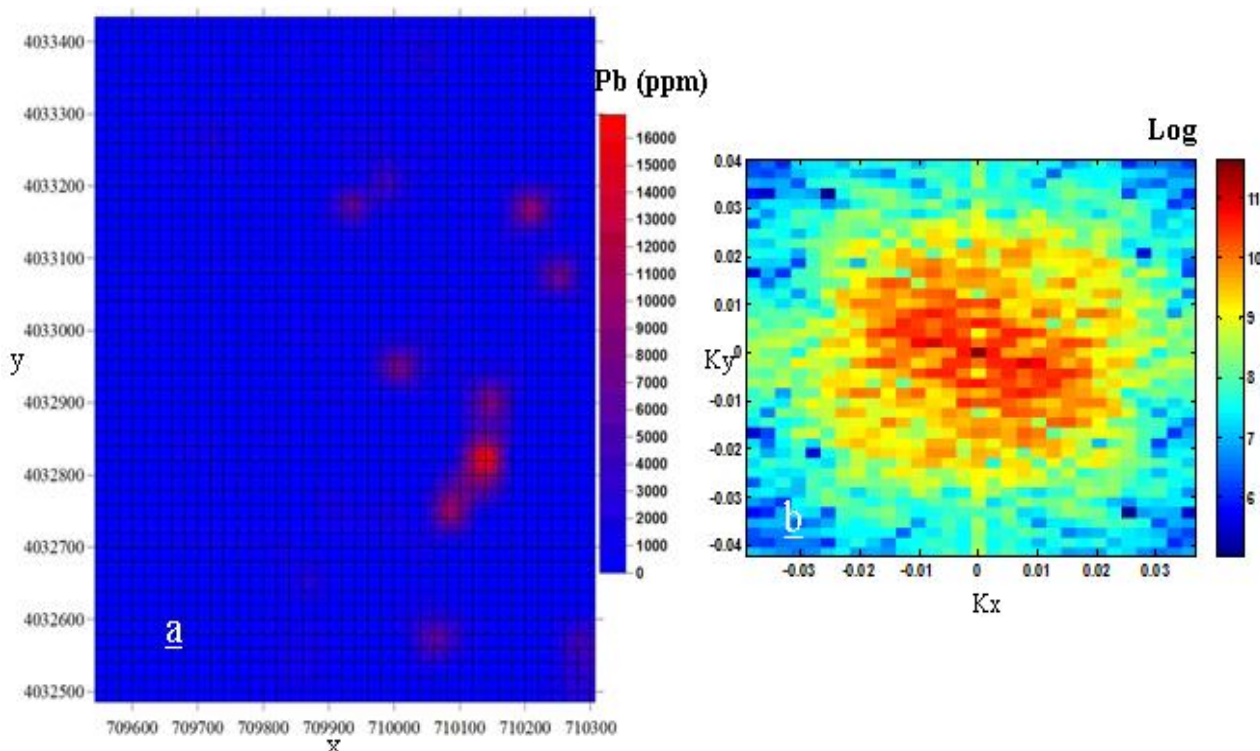


Figure 6. (a) Pb geochemical distribution map in SD (b) frequency distribution map in FD (Power-Spectrum (PS) map of Pb obtained by Fourier transformation).

Table 2. Two designed filter functions based on wave numbers and power spectrum values.

	Filter function	Frequency content	Eliminated frequencies
Frequency band 1	$G(k_x, k_y) = \begin{cases} 1 & k_x \text{ and } k_y \leq 0.01 \\ 0 & \text{otherwise} \end{cases}$	Very low frequencies	High and moderate frequencies
Frequency band 2	$G(k_x, k_y) = \begin{cases} 1 & k_x \text{ and } k_y \leq 0.005 \\ 0 & \text{otherwise} \end{cases}$	Very low frequencies	High and moderate frequencies

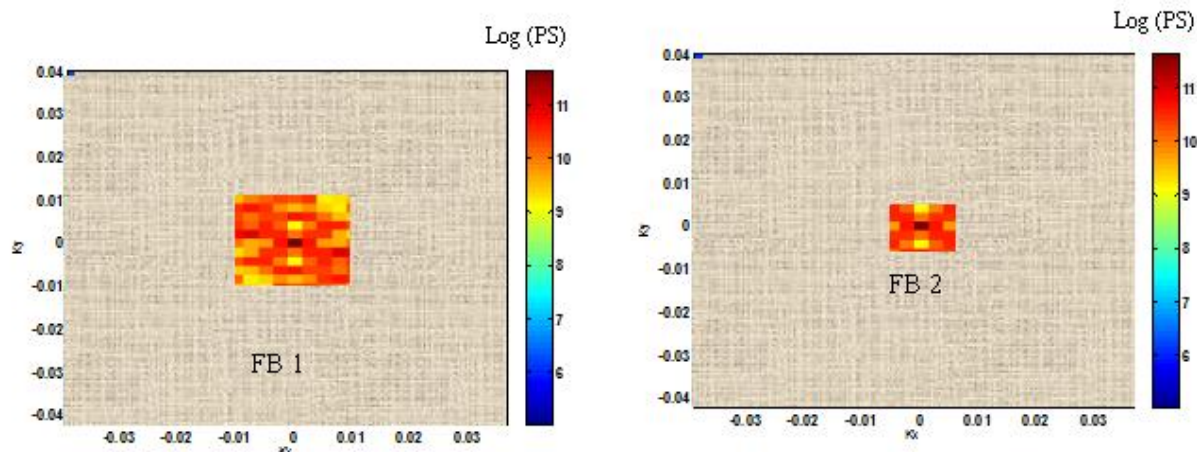


Figure 7. Power spectrum (PS) maps for FB1 and FB2 obtained from Pb GDM using 2DFT and designed filter functions.

The low-pass filters preserve the low frequencies. The low frequencies are related to the low wave number values and low variability of GDM. The filter function, $G(K_x, K_y)$, modifies the function $E(K_x, K_y)$ so that some ranges of wave numbers are eliminated and the others are enhanced. The PCA method was employed on these different FBs separately, and the mineralization factors were evaluated. The PCA method was performed on different wave numbers and their power spectrum values for 39 elements. The results obtained are shown in Table 3. In order to discriminate the elements and determine the exploratory patterns, 0.5 was considered as an evaluation criterion in rotated component matrix. The geochemical data in these FBs consists of the largest power spectrum values and the lowest frequencies.

PCA classifies the elements in these FBs into 2 principal components (PCs) (Table 3). The elements Sb, Cu, Au, Sr, Mn, As, Ca, U, Pb, Mg, Y, Zn, Ag, Mo, S, Tl, Cr, Bi, Ba, Be, Cd, Fe, W, Co, Ce, V, P, Ni, Th, Li, Sn, Rb, Cs, Al, K, and Zr are effective elements in PC1. PC2 is related to the elements Ca, U, Mg, Mo, Y, Zn, Ag, Mo, S, Tl, Cr, Bi, Ba, Be, Cd, Fe, W, Co, Ce, V, P, Ni, Th, Li, Sn, Rb, Cs, Al, K, Ti, Nb, Na, and Zr. The mineralization elements (i.e. Pb and Zn) were not properly separated from the other elements. The scores of elements in PC1 for FB 1 and 2 are illustrated in Figure 8. The mineralization and paragenesis elements were not classified properly in these bands. The mineralization and background patterns are not distinguishable in these very low FBs. The frequency behavior of the paragenesis and mineralization elements is similar to the other

elements (background pattern) in these FBs. Therefore, the frequency oscillations of Pb and Zn are similar to the frequency variations of background elements such as Ca and Mg. Hence, FDM of the elements was not affected by the deep deposit in this area. In this area, the paragenesis and mineralization elements in the surface GDM do not have a distinctive frequency pattern in low FBs, and FDMs are affected by the background that is related to the regional geological processes. The presented scenario indicates that there is a low probability about the presence of deep ore deposit in this area. The coefficients of PCs in rotated component matrix in the PCA method demonstrate that there is no frequency anomaly in FDM, which is related to the deep geochemical anomaly. These results reduce the importance and intensity of mineralization elements in the depth. The results obtained predict that there are non-mineralization zones in the depth. The results of the detailed exploration surveys and drilled borehole confirm these results. The distributions of Pb, Zn, and Fe concentrations in the borehole BH03 and the mineralized and non-mineralized zones are illustrated in Figures 9-11. There is a complete compliance between the results. There is a non-mineralized zone in the depths of 60 m up to 150 m based on the results of the drilled borehole. The geochemical anomaly in GDM is more affected by the surface and shallow mineralization zones in this area. The interpretation of FDM as a newly presented pattern recognition scenario can properly predict the importance of mineralization zones in the depth without exploratory drilling.

Table 3. Rotated component matrix in PCA method for FB 1, 2.

	FB1			FB2	
	1	2		1	2
Au	.877	.433	Au	.884	.432
Cr	.740	.669	Cr	.743	.668
Mn	.868	.490	Mn	.871	.488
Ni	.597	.800	Ni	.600	.800
Pb	.824	.495	Pb	.839	.527
Sr	.878	.471	Sr	.880	.471
Ba	.728	.676	Ba	.735	.671
Be	.721	.676	Be	.733	.665
Ti	.483	.875	Ti	.480	.877
Fe	.718	.692	Fe	.725	.687
Al	.521	.851	Al	.521	.852
Ca	.859	.505	Ca	.861	.505
Li	.556	.828	Li	.557	.828
P	.607	.794	P	.608	.794
V	.628	.777	V	.630	.776
Mg	.833	.548	Mg	.835	.548
K	.519	.854	K	.519	.855
Na	.310	.923	Na	.304	.933
S	.744	.638	S	.750	.638
Zr	.506	.847	Zr	.510	.859
Ag	.807	.529	Ag	.825	.530
As	.848	.467	As	.861	.456
Bi	.717	.664	Bi	.738	.655
Co	.682	.728	Co	.687	.726
Cu	.880	.458	Cu	.888	.452
Mo	.750	.615	Mo	.763	.623
Sb	.894	.419	Sb	.909	.407
Zn	.831	.548	Zn	.832	.551
Sn	.545	.837	Sn	.546	.838
W	.689	.717	W	.690	.722
Cs	.533	.844	Cs	.533	.845
Nb	.477	.878	Nb	.475	.880
U	.849	.522	U	.852	.521
Cd	.696	.642	Cd	.728	.637
Rb	.536	.843	Rb	.537	.844
Th	.578	.815	Th	.579	.815
Y	.830	.551	Y	.833	.550
Ce	.656	.752	Ce	.661	.748
Tl	.728	.626	Tl	.745	.638

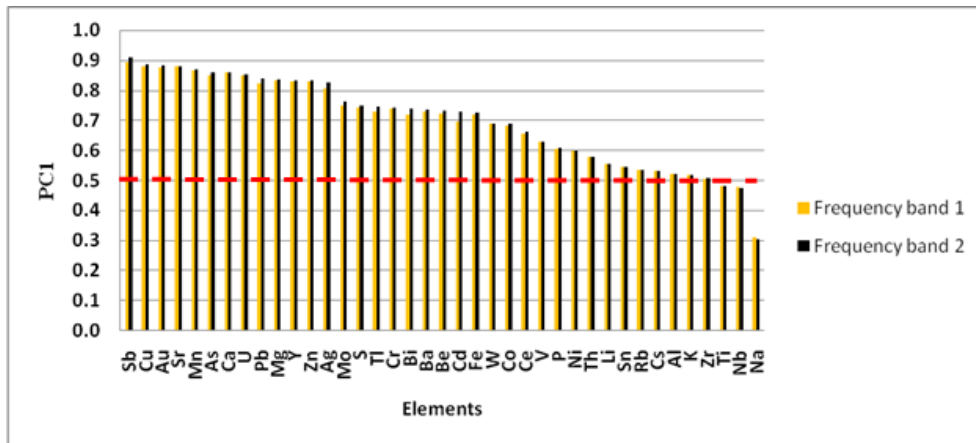


Figure 8. Scores of elements in PC1 for frequency bands 1 and 2. Mineralization and paragenesis elements have not been classified properly.

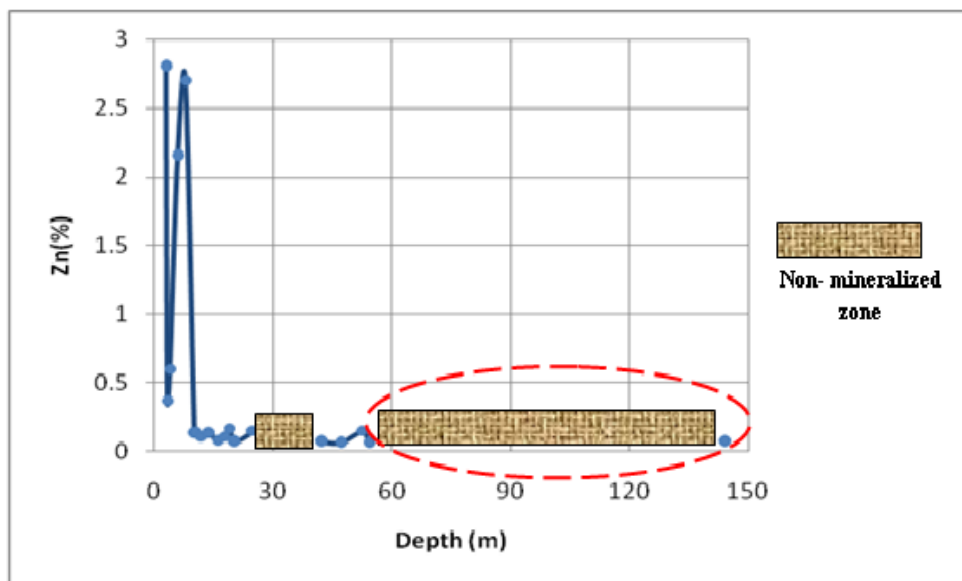


Figure 9. Concentration of Zn versus depth in borehole BH03 and non- mineralized zones.

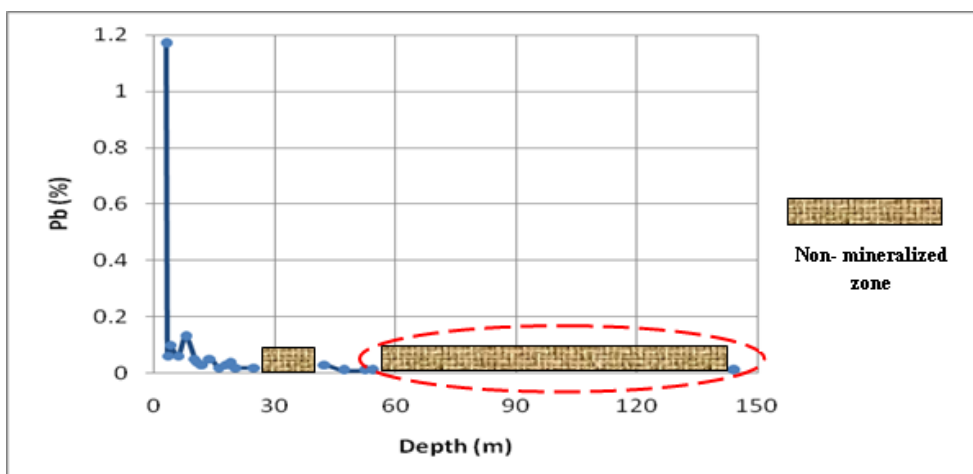


Figure 10. Concentration of Pb versus depth in borehole BH03 and non- mineralized zones.

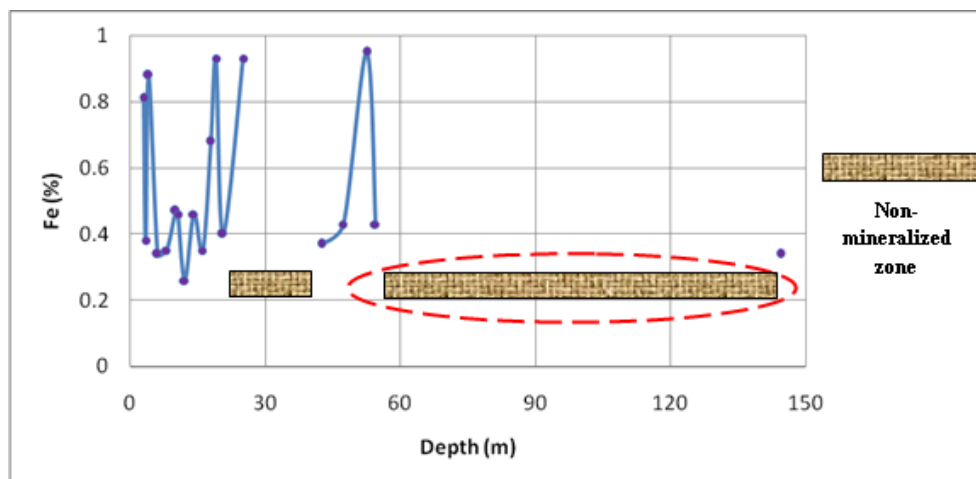


Figure 11. Concentration of Fe versus depth in borehole BH03 and non-mineralized zones.

4. Conclusions

The frequency domain of surface geochemical data can be obtained using 2DFT. This research work showed that there was an inverse relationship between the depth of ore deposit and the frequencies of surface GDM. The very low frequencies in FDM could be related to the background values and anomaly values created by very deep mineral deposits. Two low-pass filter functions were designed and applied to FDM of elements. The separated very low frequencies were analyzed using PCA. In this research work, new exploratory information was concluded using interpretation of FD that is not achievable in the spatial domain. These achievements are:

1- This proposed method can distinguish the presence or absence of Pb-Zn mineral deposits in the depth before drilling borehole.

2- The results obtained show that the Pb-Zn mineralization phase does not affect very low FBs in FDM that are related to deep ore deposit. FDMs of the paragenesis and mineralization elements are similar to the background and syngenetic elements in very low FBs. Therefore, the frequency oscillations of Pb and Zn are similar to the frequency behaviors of the background elements such as Ca and Mg. There is no mineralization phase in FDM of these FBs.

3- The introduced approach shows that the probability of the presence of Pb-Zn deep ore deposit in this area is very low. The results of FD demonstrate that there are non-mineralization zones in the depth. This fact cannot be concluded properly using the spatial domain. These results were also not confirmed by the results of concentration and mineralization in the exploration drilled borehole. There is a non-mineralized zone in the depths of 60 m up to 150 m based on the results of drilled borehole.

4- The applied method shows that the geochemical anomaly in GDM is more affected by the surface and shallow mineralization zones in this area.

Therefore, the presented method is an effective pattern recognition approach for decomposing mixed geochemical populations and identifying deep mineral deposits without exploratory drilling.

References

- [1]. Carranza, E.J.M. and Sadeghi, M. (2012). Primary geochemical characteristics of mineral deposits- Implications for exploration. *Ore Geology Reviews*. 45: 1-4.
- [2]. Safronov, N.I. (1936). Dispersion haloes of ore deposits and their use in exploration. *Probl. Sov. Geol.* 4: 41-53.
- [3]. Govett, G.J.S. (1983). *Rock geochemistry in mineral exploration: Handbook of exploration geochemistry*, V. 3. Elsevier. Amsterdam. 461 P.
- [4]. Goldberg, I.S., Abramson, G.Y. and Los, V.L. (2003). Depletion and enrichment of primary haloes: their importance in the genesis of and exploration for mineral deposits. *Geochemistry: Exploration, Environment, Analysis*, 3 (3): 281-293.
- [5]. Bierlein, F.P., Fuller, T., Stüwe, K., Arne, D.C. and Keays, R.R. (1998). Wallrock alteration associated with turbidite-hosted gold deposits. Examples from the Palaeozoic Lachlan Fold Belt in central Victoria, Australia. *Ore Geology Reviews*. 13 (1): 345-380.
- [6]. Lovering, T.S. (1949). *Rock Alteration as a Guide to Ore- East Tintic District, Utah*. Economic Geology Monograph 1. Economic Geology Publishing Co., Urbana. Illinois. 64 P.
- [7]. Hannington, M.D., Santaguida, F., Kjarsgaard, I.M. and Cathles, L.M. (2003). Regional-scale hydrothermal alteration in the Central Blake River Group, western Abitibi subprovince, Canada:

implications for VMS prospectivity. *Miner. Deposita*. 38: 393-422.

[8]. Grigorian, S.V. (1985). *Secondary Lithochemical Haloes in Prospecting for Hidden Mineralization*. Nedra Publishing House, Moscow. 176 P. (In Russian).

[9]. Grigorian, S.V. (1992). *Mining Geochemistry*. Nedra Publishing House. Moscow.

[10]. Ziiai, M., Pouyan, A.A. and Ziaei, M. (2009). Neuro-fuzzy modelling in mining geochemistry: Identifications of geochemical anomalies. *Journal of Geochemical Exploration*. 100 (1): 25-36.

[11]. Levinson, A.A. (1980). *Introduction to Exploration Geochemistry*. Applied Publishing Ltd., Wilmette. USA.

[12]. Ziiai, M., Abedi, A. and Ziaei, M. (2007). Prediction of hidden ore bodies by new integrated computational model in marginal Lut region in east of Iran. In: Milkereit, B. (Ed.), *Proc. Exploration 07: Fifth Decennial Internat. Conf. Mineral Exploration*. Toronto. Canada, pp. 957-961.

[13]. Ziiai, M., Carranza, E.J.M. and Ziaei, M. (2011). Application of geochemical zonality coefficients in mineral prospectivity mapping. *Comput. Geosci*. 37: 1935-1945.

[14]. Ziiai, M., Doulati, F., Ziaei, M. and Soleymani, A.A. (2012). Neuro-fuzzy modeling based genetic algorithms for identification of geochemical anomalies in mining geochemistry. *J. Applied Geochemistry*. 27: 663-676.

[15]. Goodell, P.C. and Petersen, U. (1974). *Julcani mining district, Peru: a study of metal ratios*. *Econ. Geol.* 69: 347-361.

[16]. Jones, B.K. (1992). Application of metal zoning to gold exploration in porphyry copper systems. *J. Geochem. Explor.* 43: 127-155.

[17]. Pirajno, F. and Smithies, R.H. (1992). The FeO/(FeO+MgO) ratio of tourmaline: a useful indicator of spatial variations in granite-related hydrothermal mineral deposits. *J. Geochem. Explor.* 42: 371-381.

[18]. Shahi, H., Ghavami, R., Kamkar Rouhani, A. and Asadi-Haroni, H. (2014). Identification of mineralization features and deep geochemical anomalies using a new FT-PCA approach. *Journal of Geopersia*. 4 (2): 101-110.

[19]. Shahi, H., Ghavami, R., Kamkar Rouhani, A. and Asadi-Haroni, H. (2015). Application of Fourier and wavelet approaches for identification of geochemical anomalies. *Journal of African Earth Sciences*. 106: 118-128.

[20]. Shahi, H., Ghavami, R. and Kamkar Rouhani, A. (2016). Detection of deep and blind mineral deposits using new proposed frequency coefficients method in frequency domain of geochemical data. *Journal of Geochemical Exploration*. 162: 29-39.

[21]. Heideman, M.T., Johnson, D.H. and Burrus, C.S. (1984). Gauss and the history of the fast Fourier transform. *IEEE ASSP Magazine*. 1 (4): 14-21

[22]. Afzal, P., Fadakar Alghalandis, Y., Moarefvand, P., Rashidnejad Omran, N. and Asadi Haroni, H. (2012). Application of power-spectrum-volume fractal method for detecting hypogene, supergene enrichment, leached and barren zones in Kahang Cu porphyry deposit, Central Iran. *Journal of Geochemical Exploration*. 112: 131-138.

[23]. Afzal, P., Harati, H., Fadakar Alghalandis, Y. and Yasrebi, A.B. (2013). Application of spectrum-area fractal model to identify of geochemical anomalies based on soil data in Kahang porphyry-type Cu deposit, Iran. *Chemie der Erde*. 73: 533-543.

[24]. Cao, L. and Cheng, Q. (2012). Quantification of anisotropic scale invariance of geochemical anomalies associated with Sn-Cu mineralization in Gejiu, Yunnan Province, China. *Geochemical Exploration*. 122: 47-54.

[25]. Cheng, Q. and Zhao, P. (2011). Singularity theories and methods for characterizing mineralization processes and mapping geo-anomalies for mineral deposit prediction. *Geoscience Frontiers*. 2 (1): 67-79.

[26]. Hassani, H., Daya, A. and Alinia, F. (2009). Application of a fractal method relating power spectrum and area for separation of geochemical anomalies from background. *Aust J Basic Appl Sci*. 3 (4): 3307-3320

[27]. Cheng, Q. (1999). Spatial and scaling modelling for geochemical anomaly separation. *Journal of Geochemical Exploration*. 65: 175-194.

[28]. Cheng, Q., Xu, Y. and Grunsky, E. (2000). Integrated Spatial and Spectrum Method for Geochemical Anomaly Separation. *Natural Resources Research*. 9 (1): 43-52.

[29]. Zuo, R. (2011). Identifying geochemical anomalies associated with Cu and Pb-Zn skarn mineralization using principal component analysis and spectrum-area fractal the Gangdese Belt, Tibet (China). *J. Geochemical Exploration*. 111: 13-22.

[30]. Zuo, R. (2011). Decomposing of mixed pattern of arsenic using fractal model in Gangdese belt, Tibet, China. *Applied Geochemistry*. 26: S271-S273.

[31]. Zuo, R., Carranza, E.J.M. and Cheng, Q. (2012). Fractal/multifractal modelling of geochemical exploration data. *Journal of Geochemical Exploration*. 122: 1-3.

[32]. Zuo, R., Xia, Q. and Zhang, D. (2013). A comparison studies of the C-A and S-A models with singularity analysis to identify geochemical anomalies in covered areas. *Applied Geochemistry*. 33: 165-172.

[33]. Wang, H. and Zuo, R. (2015a). A comparative study of trend surface analysis and spectrum-area

multifractal model to identify geochemical anomalies. *Journal of Geochemical Exploration*. 155: 84-90.

[34]. Wang, J., and Zuo, R. (2015). A MATLAB-based program for processing geochemical data using fractal/multifractal modeling. *Earth Science Informatics*. 8 (4): 937-947.

[35]. Cheng, Q. (2012). Singularity theory and methods for mapping geochemical anomalies caused by buried sources and for predicting undiscovered mineral deposits in covered areas. *Journal of Geochemical Exploration*. 122: 55-70.

[36]. Farzamian, M., Kamkar Rouhani, A., Yarmohammadi, A., Shahi, H., Sabokbar, H.F. and Ziaie, M. (2016). A weighted fuzzy aggregation GIS model in the integration of geophysical data with geochemical and geological data for Pb-Zn exploration in Takab area, NW Iran. *Arabian Journal of Geosciences*. 9 (2): 1-17.

[37]. Saki, A. (2010). Proto-Tethyan remnants in northwest Iran: geochemistry of the gneisses and metapelitic rocks. *Gondwana Research*. 17 (4): 704-714.

[38]. Elias, S. and Shakarchi, R. (2003). *Fourier Analysis: An introduction*, ed.

[39]. Gallagher, T.A., Nemeth, A.J. and Hacein-Bey, L. (2008). An introduction to the Fourier transform: Relationship to MRI. *American journal of roentgenology*. 190 (5): 1396-1405.

[40]. Van Loan, C. (1992). *Computational frameworks for the fast Fourier transform*. Society for Industrial and Applied Mathematics.

[41]. Gallagher, T.A., Nemeth, A.J. and Hacein-Bey, L. (2008). An introduction to the Fourier transform: relationship to MRI. *American journal of roentgenology*. 190 (5): 1396-1405.

[42]. Cios, K.J., Pedrycz, W., Swiniarski, R.W. and Kurgan, L. (2007). *Data Mining: A Knowledge Discovery Approach*. Springer. US. pp. 9-24.

[43]. Dobrin, M.B. and Savit, C.H. (1988). *Geophysical prospecting*: McGraw-Hill Book Co., New York, 867 P.

[44]. Bhattacharyya, B.K. (1966). Continuous spectrum of the total-magnetic-field anomaly due to a rectangular prismatic body. *Geophysics*. 31 (1): 97-121.

[45]. Gonzalez, R.C. and Woods, R.E. (2002). *Digital image processing*. Prentice-Hall, Upper Saddle River, NJ, 793 P.

[46]. Ge, Y., Cheng, Q. and Zhang, S. (2005). Reduction of edge effects in spatial information extraction from regional geochemical data: a case study based on multifractal filtering technique. *Computers & Geosciences*. 31: 545-554.

[47]. Cheng, Q., Jing, L. and Panahi, A. (2006). Principal component analysis with optimum order sample correlation coefficient for image enhancement. *International Journal of Remote Sensing*. 27 (16): 3387-3401.

[48]. Cheng, Q., Xu, Y. and Grunsky, E. (1999). Integrated spatial and spectral analysis for geochemical anomaly separation, August 6-11. In 6th Annual Conference of the International Association for Mathematical Geology. Trondheim, Norway. pp. 87-92.

[49]. Jolliffe, I. (2002). *Principal component analysis*. John Wiley & Sons, Ltd.

[50]. Rencher, A.C. (2002). *Principal component analysis. Methods of Multivariate Analysis*. Second Edition. pp. 380-407.

[51]. Cheng, Q., Bonham-Carter, G., Wang, W., Zhang, S., Li, W. and Xia, Q. (2011). A spatially weighted principal component analysis for multi-element geochemical data for mapping locations of felsic intrusions in the Gejiu mineral district of Yunnan, China. *Computer & Geosciences*. 37: 662-669.

[52]. Loughlin, W.P. (1991). Principal component analysis for alteration mapping. *Photogrammetric Engineering and Remote Sensing*. 57 (9): 1163-1169.

[53]. Davis, J.C. (2002). *Statistics and Data Analysis in Geology*. 3rd ed. JohnWiley&Sons Inc., NewYork, 550P.

[54]. Yousefi, M., Kamkar-Rouhani, A. and Carranza, E.J.M., (2012). Geochemical mineralization probability index (GMPI): a new approach to generate enhanced stream sediment geochemical evidential map for increasing probability of success in mineral potential mapping. *Journal of Geochemical Exploration*. 115: 24-35.

پیش‌بینی زون کانی‌سازی پراکنده در عمق با استفاده از حوزه فرکانس داده‌های ژئوشیمیایی سطحی

حسین شاهی

گروه مهندسی معدن، دانشگاه گناباد، ایران

ارسال ۲۰۱۶/۸/۲، پذیرش ۲۰۱۷/۵/۵

نویسنده مسئول مکاتبات: hssn.shahi@gmail.com

چکیده:

تمایز بین ذخایر کانی‌سازی پنهان و کانی‌سازی پراکنده یکی از چالش‌های مهم در بخش ژئوشیمی اکتشافی است. حوزه فرکانس (FD) داده‌های ژئوشیمیایی سطحی می‌تواند این مشکل را حل کند. دستیابی به این اطلاعات جدید اکتشافی در حوزه مکان غیرممکن ولی با استفاده از تفسیر حوزه فرکانس داده‌های ژئوشیمیایی قابل دستیابی است. در این تحقیق، به منظور تجزیه الگوهای پیچیده ژئوشیمیایی مرتبط با ذخایر معدنی، حوزه فرکانس داده‌های ژئوشیمیایی مورد تجزیه و تحلیل قرار گرفته است. به منظور شناسایی منطقه کانی‌سازی پراکنده سرب و روی در محدوده چیچکلو، یک روش جدید بر اساس ترکیب روش‌های تبدیل فوری دو بعدی (2DFT) و روش تحلیل مؤلفه‌های اصلی (PCA) پیشنهاد داده شده است. داده‌های ژئوشیمیایی سطحی با استفاده از تبدیل فوری دو بعدی به حوزه فرکانس تبدیل می‌شود؛ سپس دو فیلتر پایین‌گذر طراحی و بر روی داده‌های حوزه فرکانس اعمال شده است. روش تحلیل مؤلفه‌های اصلی بر روی این باندهای فرکانسی به صورت مجزا انجام می‌گیرد. این روش پیشنهادی به طور مناسبی ارتباط بین فرکانس‌های پایین در نقشه توزیع ژئوشیمیایی سطحی (GDM) و ذخایر عمیق را نشان می‌دهد. اطلاعات به دست آمده از اکتشافات تفصیلی و حفاری‌های اکتشافی از قبیل گمانه‌ها، نتایج حاصل از این روش را تأیید می‌کنند. این روش ترکیبی جدید یک ابزار ارزشمند پردازش داده و یک روش تشخیص الگو در اکتشافات ژئوشیمیایی است. این روش در مقایسه با روش‌های سنتی اکتشاف کاملاً ارزان‌تر است.

کلمات کلیدی: حوزه فرکانس داده ژئوشیمیایی، تحلیل مؤلفه‌های اصلی، تبدیل فوری، منطقه کانی‌سازی پراکنده، تشخیص الگو.